Tunneling magnetoresistance with amorphous electrodes

Martin Gradhand,[1,2,*] Christian Heiliger,[3,4,†] Peter Zahn,[2] and Ingrid Mertig[2,1]

[1] *Max-Planck-Institut für Mikrostrukturphysik, Weinberg 2,06120 Halle, Germany*
[2] *Fachbereich Physik, Martin-Luther-Universität Halle-Wittenberg, D-06099 Halle, Germany*
[3] *Center for Nanoscale Science and Technology, National Institute of Standards and Technology, Gaithersburg, MD 20899-6202*
[4] *Maryland NanoCenter, University of Maryland,College Park, MD, 20742*

(Dated: September 13, 2007)

A detailed first principles analysis of the transport properties of different magnetic electrode materials for MgO tunnel junctions is performed to elucidate the microscopic origin of the TMR effect. The spin-dependent transport properties of the magnetic materials are analyzed separately from the particular interface geometry with the tunneling barrier. We use the bulk properties of the barrier to identify the important tunneling states. For MgO these are Δ_1-like states. From the analysis of this effective spin polarization we can predict the potential of certain magnetic materials to create a high TMR ratio in a tunnel junction.This polarization is as high as 98 % and 86 % for Fe and Co, respectively for only a few monolayers, but very small and negative, -7 %, for amorphous Fe. This explains the finding that for crystalline Co and Fe one monolayer next to the MgO barrier is sufficient to reach TMR ratios higher than 500 % independent of whether the crystalline monolayer is coupled to a non-magnetic or to an amorphous lead. However, in direct contact with MgO amorphous Fe reduces the TMR ratio drastically to 44 %.

PACS numbers: 73.63.-b,72.15.Cz,71.23.-k,85.30.Mn

The effect of tunneling magnetoresistance (TMR) has been a focus of research since its rediscovery by Moodera et al.[1] and Miyazaki et al.[2] in 1995. Julliere[3], who analyzed this effect in 1975, observed that the tunneling current through a layered system consisting of two ferromagnetic electrodes separated by an insulating barrier depends on the relative orientation of the magnetization of the ferromagnetic layers to each other. Different currents are measured for parallel (P) and for antiparallel (AP) alignment of the lead magnetizations. To quantify this effect different TMR ratios are defined in the literature. The most common one is the optimistic TMR ratio given by

$$\frac{R_{AP}-R_P}{R_P}=\frac{g_P-g_{AP}}{g_{AP}}\ , \tag{1}$$

where g_P (R_P) and g_{AP} (R_{AP}) are the conductances (resistances) in the parallel and antiparallel configuration. Typical applications exploiting the TMR effect are hard disk read heads[4,5] and magnetic random access memories (MRAM).[6,7] Three properties of a tunnel junction are important for industrial usage. First, a high TMR ratio is necessary. Second, the tunnel junction has to have a practicable signal to noise ratio and third, the device design has to allow for a large-scale production at low costs. In the last decade the TMR ratio of tunnel junctions with crystalline MgO barriers was increased remarkably and reached values above 300 %[8–11] at room temperature. In contrast, the values for systems with amorphous aluminum oxide (Al_2O_3) barriers are still less than 100 %.[12,13] In theoretical investigations of systems with crystalline MgO barriers TMR ratios beyond 1000 % were predicted.[14,15] The discrepancy between experimental and theoretical results could be explained in terms of structural imperfections in the experimental systems in contrast to the ideal systems of the theoretical investigations. Further structural analysis[9,16,17] of tunnel junctions showed that even with partial structural disorder in the magnetic layers consisting of CoFeB, a TMR ratio of 230 %[16] is realizable. In addition, a crystalline magnetic CoFe layer forms between the MgO barrier and the otherwise amorphous electrode under the influence of annealing.[9] Recent *ab initio* calculations used semi-infinite ideal leads but do not consider partial structural disorder and finite thickness of the ferromagnetic electrode layers.[14,15,18–23] Only disorder at the Fe/MgO interface[18,23] or in the MgO barrier[24] was analyzed. The aim of this article is to present a detailed discussion of the microscopic origin of tunneling under the influence of structural disorder and finite thickness of the ferromagnetic electrodes. In the present paper we expand on our earlier analysis[25] and consider additional lead materials.

In this work three important experimental results concerning the structure of a tunnel junction are taken into account as sketched in Fig. 1. First, the tunnel junction is embedded between semi-infinite non-magnetic reservoirs to account for the finite thicknesses of the magnetic layers. Second, we include a layer with structural disorder represented by amorphous iron (a-Fe). Third, there is a crystalline magnetic layer of finite thickness next to the barrier represented by a finite number of Fe or Co monolayers in a bcc structure.

The paper is organized as follows. After a short introduction of our theoretical methods, the following sections are separated in two parts. The first part (Sec. II) covers the results of the amorphous iron. In particular, the atomic structure simulation, the electronic and magnetic structure calculation, and the analysis of the transport properties of amorphous iron is discussed in this part.

The second part of the article includes all sections con-

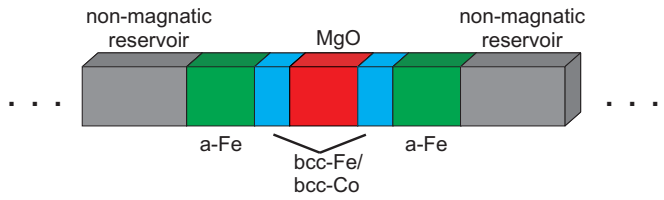

FIG. 1: Schematic structure of the investigated tunnel junctions

cerning the TMR effect. In Sec. III we review the basic principles of the microscopic origin of the TMR effect. We extend this part by the introduction of special spin polarizations of the current (P_{Δ_1} and P_{eff}) to discuss the potential of different magnetic materials to lead to high TMR ratios in a tunnel junction with crystalline MgO in the following section. In addition we present results of conductance calculations of different magnetic materials embedded between non-magnetic reservoirs to analyze the different current polarizations. As magnetic materials we consider crystalline iron (bcc-Fe), cystalline cobalt in a iron structure (bcc-Co) and amorphous iron (a-Fe). In section V we compare these results to our *ab initio* calculations of tunnel junctions using these magnetic materials.

I. METHODS

The theoretical method used for the electronic structure calculation is a screened Kohn-Korringa-Rostoker (KKR) Green's function method.[26,27] It is based on density functional theory (DFT) in the local spin density approximation (LSDA). The magnetic moments are forced to be collinear. For the conductance calculations the Baranger-Stone formalism[28] in the KKR Green's function expression[29] was used. This formalism is equivalent to the Landauer approach[30] and the conductance is expressed in the zero bias limit as

$$g = g_0 \sum_\sigma T^\sigma = g_0 \sum_\sigma \int d^2k_\parallel T^\sigma(\mathbf{k}_\parallel),$$
$$g_{P(AP)} = g^{\uparrow\uparrow(\uparrow\downarrow)} + g^{\downarrow\downarrow(\downarrow\uparrow)}, \qquad (2)$$

where T^σ is the spin-dependent transmission probability, $g_0 = e^2/h$ denotes the universal conductance quantum, and σ is the spin index. The in-plane wave vector $\mathbf{k}_\parallel$ is used because of the translational invariance parallel to the interface. The integration has to be performed over the surface Brillouin zone. The transmission, which is energy dependent in general, has to be taken at the common Fermi level. The spin-dependent conductance in the parallel magnetic configuration of the tunnel junction is labeled by $g^{\uparrow\uparrow}$ and $g^{\downarrow\downarrow}$ for the majority and minority spin channel, respectively. For the antiparallel configuration the conductances are labeled $g^{\uparrow\downarrow}$ and $g^{\downarrow\uparrow}$. For the conductance calculations the structure was embedded between non-magnetic semi-infinite leads to account for the open boundary conditions. This is done by the decimation technique implemented in the KKR code.[31,32]

II. AMORPHOUS IRON

In this section we present the results of the structural simulation and the corresponding electronic properties of amorphous Fe (a-Fe). In addition, we show that a-Fe is an ohmic conductor on the analyzed lengthscale. There have been a number of experimental investigations of amorphous Fe.[33–40] Since the structure is not stable as bulk phase it was investigated as a thin film[34,35], or stabilized by Co and B impurities[33,40], or as a substitutional alloy with B.[39] Therefore, the experimental results differ strongly. For example, the average magnetic moment ranges between 1.0 μ_B and 1.5 μ_B. *ab initio* electronic structure calculations of a-Fe are rare[41–45] since typical *ab initio* methods are well suited for crystalline systems but not for the description of amorphous materials. A possible way to treat amorphous systems is the supercell method. The numerical expense of this procedure is high and restricts the size of the supercells.

To describe the atomic short range order of a-Fe the pair correlation function

$$G(r) = \frac{1}{\overline{N}} \frac{N(r)}{4\pi r^2 \Delta r} \qquad (3)$$

is used[34,35,40], where $\overline{N}$ is the average particle density, and $N(r)$ the number of atoms in the spherical shell between r and $r + \Delta r$, if one atom is situated in the center of the sphere. For comparison we use the experimentally obtained pair correlation function from the analysis of a thin film[34] with a density similar to the crystalline system (7.9 g cm^{-3}). The calculated pair correlation function of large periodic systems containing 16 to 108 atoms per unit cell was fitted to the experimental one by a Monte-Carlo algorithm. Fig. 2 shows G(r) of a supercell of 16, 27, and 108 atoms in comparison to the experimental result given by Ichikawa.[34] We conclude that a supercell with 16 atoms is well suited to describe the structural properties of the amorphous system up to the third-nearest neighbor shell in agreement with other theoretical investigations.[41] Therefore, we use this supercell in our electronic structure calculations.

Fig. 3 compares the calculated density of states (DOS) of the supercell with 16 atoms with the DOS of crystalline bulk Fe. The main features of the DOS of bulk Fe are broadened because of the structural disorder and the weights at the Fermi level are changed. These results are in very good agreement with the calculations of Turek et al.[42] who used a larger supercell with 64 atoms. The conductance is determined by the states at the Fermi level and it can be concluded from the DOS that the transport properties of a-Fe will be different from that of crystalline Fe.

The average magnetic moment of a-Fe is 1.7 μ_B which is in fairly good agreement with the experimental results

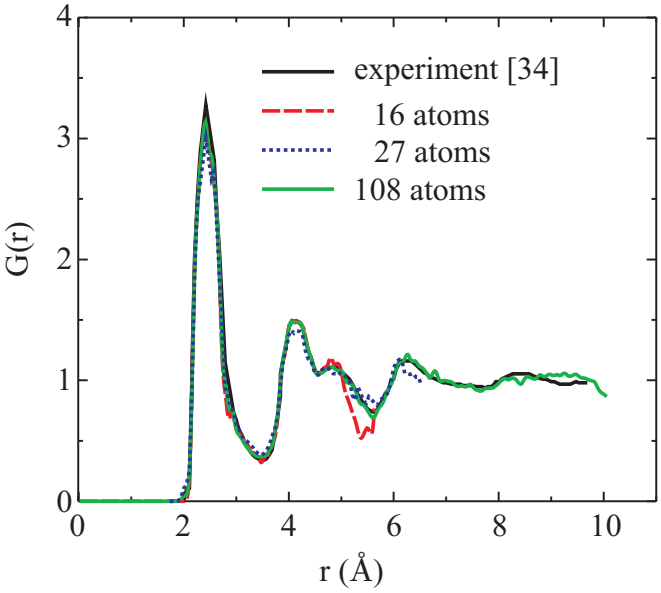

FIG. 2: Calculated pair correlation function G(r) for supercells with 16, 27, and 108 atoms in comparison with an experimental one[34]

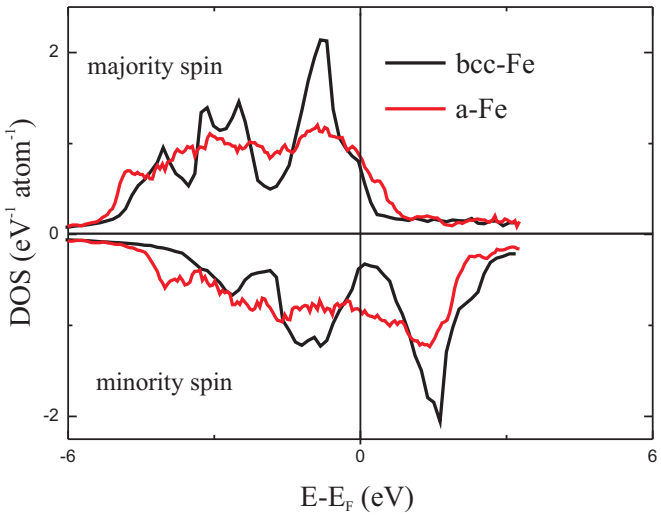

FIG. 3: Calculated spin-dependent DOS for amorphous Fe (a-Fe) simulated by a supercell with 16 atoms in comparison with bcc-bulk Fe

and the calculations by Turek et al.[42] who found 1.3 μ_B. In Fig. 4 the distribution of the local magnetic moments is presented. The collinear magnetic ground state is characterized by moments around 2 μ_B and only a few negative magnetic moments which agrees with the results of Turek et al.[42] and is comparable to non-collinear calculations.[41,43,44] Although the averaged magnetic moments in collinear and non-collinear configurations are quite similar[41,43,44] the transport properties can differ significantly[46] and have to be investigated separately.

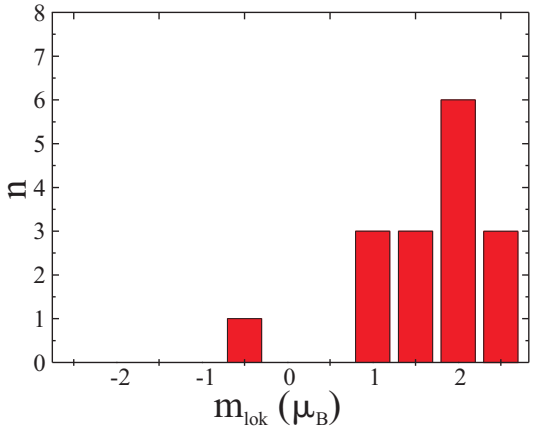

FIG. 4: Histogram of the local magnetic moments of amorphous Fe (a-Fe) within a supercell of 16 atoms

For the calculations of the electronic transport through amorphous Fe, the potential of an amorphous layer with 5 a_{Fe} thickness was calculated self-consistently in a supercell where a_{Fe}=2.87 Å is the lattice constant of crystalline Fe. First of all, the conductance through this cell embedded between semi-infinite crystalline Fe electrodes was computed. The insertion of the amorphous layer decreases the conductance of pure crystalline Fe. Fig. 5 shows the conductance map $T(\mathbf{k}_{\|})$ of both spin channels for the crystalline Fe in comparison to the system with one and seven amorphous layers. The Brillouin zone (BZ) in this representation is determined by the in-plane dimension of the supercell (2 a_{Fe} × 2 a_{Fe}). The existence of an in-plane BZ is an artifact of the supercell description and does not exist for a real amorphous system. Nevertheless, the analysis of this artificial BZ reveals the underlying physics. The arguments of Sec. V will be even stronger for a real amorphous system which has a vanishing BZ. The structural disorder of the supercell leads to a broadening of the well defined integer transmission values of the crystalline system given by the number of Bloch states at a certain $\mathbf{k}_{\|}$-point. For the amorphous structure the contributions are non-integer values which is expected since the matching is disturbed with respect to the crystalline system by structural disorder.

In a next step we calculate the thickness dependence of the resistance given by the inverse conductance (R=1/g). No thickness dependence exists for a pure crystalline system without interfaces since the number of Bloch states is conserved and only the Sharvin resistance (R_0) is obtained.[30] Structural disorder should, however, cause a thickness dependence of the resistance. To reduce the numerical effort n cells of the self consistent potential of the amorphous supercell were embedded between semi-infinite crystalline Fe electrodes. The results presented in Fig. 6 show that the resistance area product for both spin channels increases nearly linear with increasing number of amorphous layers on this length scale. The same behavior is obtained for the total resistance area prod-

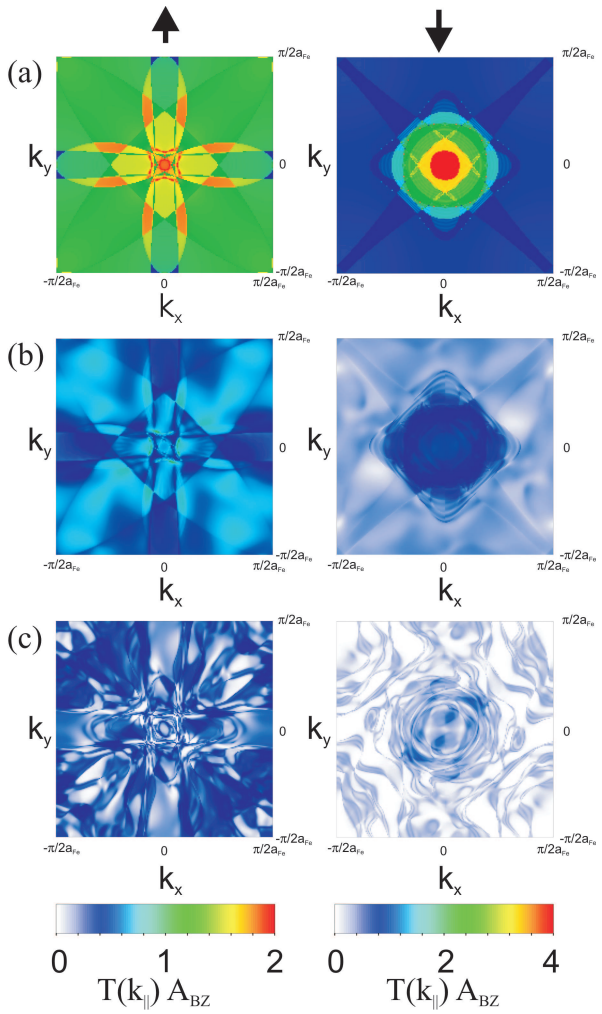

FIG. 5: Spin-dependent conductance maps $T^{\sigma}(k_{\|})$ of crystalline Fe (a), with one (b), and seven (c) layers of amorphous iron embedded between crystalline Fe

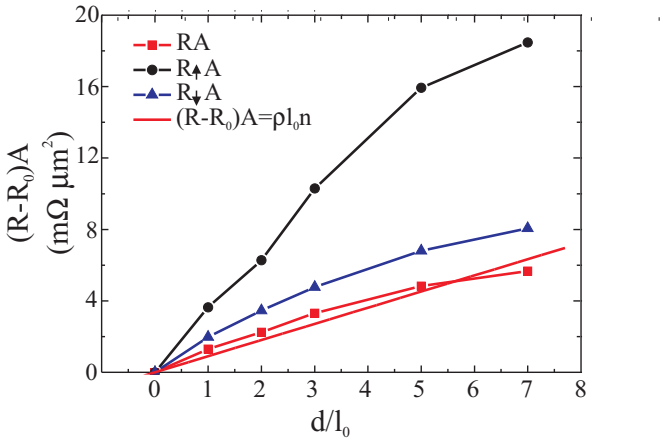

FIG. 6: Thickness dependence of the resistance area product (RA) of amorphous Fe embedded between semi-infinite bcc-Fe electrodes (thickness of one amorphous cell $l_0 = 5\ a_{\mathrm{Fe}}$, R_0 the Sharvin resistance[30], and ρ the resistivity)

uct. Fitting a linear function to the calculated values the resistivity ρ is given by 0.6 $\mu\Omega$ m, which is in good agreement with experimental values of 1 $\mu\Omega$ m.[35–37]

The conclusion of this section is that a small supercell of 16 atoms is large enough to describe the main properties of amorphous Fe. Within this length scale this material represents an ohmic conductor with a calculated resistivity comparable to experimental results. The contributions $T^{\sigma}(k_{\|})$ in the conductance map are broadened with respect to crystalline Fe by structural disorder. In the following we will use this material to introduce structural disorder in magnetic tunnel junctions.

III. BASIC PRINCIPLES

In this section we review the current understanding of the TMR effect. For this purpose we summarize briefly two different approaches to describe the TMR effect.

The first approach is the Julliere model[3] which is only valid in the diffusive limit of transport. In this model the spin polarization ($P = \frac{n_{\uparrow} - n_{\downarrow}}{n_{\uparrow} + n_{\downarrow}}$) of the density of tunneling states in the electrodes is used to estimate the TMR ratio, where $n_{\uparrow}$ and $n_{\downarrow}$ are usually approximated by the density of states at the Fermi level for majority and minority electrons, respectively. Using Eq. (1) the TMR ratio is given by

$$\frac{2P^2}{1 - P^2} \tag{4}$$

assuming identical leads. Typical spin polarizations of tunneling currents for ferromagnetic materials through an Al_20_3 barrier into a superconducting electrode are limited to values of 44 %[47,48] which causes a TMR ratio of less than 50 %. This is the case for tunnel junctions with amorphous barriers. However, the MgO barrier can be grown epitaxially and in this case the spin polarizations of Fe only can not be used. The important states for the tunneling current through crystalline MgO have to be selected. Parkin et al. have performed measurements for the polarizations of tunneling currents through crystalline MgO into a superconducting electrode and have found polarizations as high as 74 % and 85 % for Fe and CoFe as the magnetic electrode, respectively.[17] From these values a quiet high TMR ratio up to 520 % is derived within the Julliere model.

In contrast, theoretical predictions for systems with crystalline MgO barriers are even higher than 1000 %.[14,15] For the explanation of such high values coherent tunneling through the MgO barrier has to be considered. As Butler et al.[15] and Heiliger et al.[49] discussed the complex band structure of MgO leads to a symmetry selection of the barrier. Only Δ_1-like states (states with Δ_1 symmetry at the $\bar{\Gamma}$ point) around the center of the BZ can tunnel effectively through the barrier while states with other symmetry character experi-

ence a stronger damping by the MgO. A high TMR effect is expected if the electrodes transform the symmetry selection of the barrier via their exchange splitting into a spin-filtering effect. The ideal case would be to have Δ_1-like states around the center of the BZ for one spin channel only. Therefore, it is illustrative to analyze the $\mathbf{k}_\parallel$-resolved transmission probability $T^\sigma(\mathbf{k}_\parallel)$ through the magnetic materials for this property.

The details of the conductance maps $T^\sigma(\mathbf{k}_\parallel)$ for a real tunnel junction depend on the interface between the magnetic electrodes and the barrier. Even relatively small changes of the interface structure can influence the corresponding tunneling states strongly.[21]

However, to prove the ability of a magnetic system to serve as a lead material in combination with the MgO barrier in a tunnel junction, an analysis that combines the Julliere model with the symmetry selection of the barrier is useful. This means first, to restrict the polarization in the Julliere model to the current-carrying Δ_1-like states (P_{Δ_1}) and second, to restrict the analysis to states close to the center of the BZ (P_{eff}). The latter point takes into account that only states around the center of the BZ contribute to the tunneling current through a MgO barrier.

To estimate the size of the effective tunneling region around the BZ center, one has to analyze the complex band structure of MgO as done by Butler et al.[15] and Heiliger et al. .[49] The transmission probability $T(d)$ at a thickness d is determined by the imaginary part of the complex wave vector in the transport direction $Im(k_\perp)$. The band with the smallest imaginary part is the Δ_1-like band. In combination with the well known expression

$$T(d) \propto e^{-2Im(k_\perp)d} \tag{5}$$

for the transmission probability through a tunneling barrier the area contributing to the tunneling current can be estimated.

Fig. 7 shows the $\mathbf{k}_\parallel$ dependence of the transmission probability through 6 monolayers of MgO for the Δ_1-like band. The black ring indicates the region were 94 % of the transmission occurs and has the radius of $0.1\frac{2\pi}{a_{\text{Fe}}}$. The effective polarization P_{eff} is calculated in this region.

Both polarizations P_{Δ_1} and P_{eff} can be used to estimate the TMR ratio in the Julliere model and the best magnetic material can be selected. This analysis may be applied to any crystalline barrier material provided that the important tunneling states are known.

IV. TRANSPORT PROPERTIES OF POSSIBLE ELECTRODE MATERIALS

In the following we apply the analysis described in the last section to estimate the ability of three different magnetic materials to create a high TMR ratio in FM/MgO/FM tunnel junctions. One is crystalline bcc iron (bcc-Fe) which will be compared with amorphous

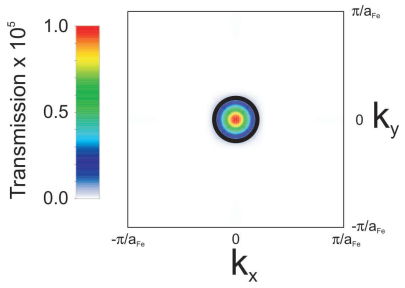

FIG. 7: Transmission probability for 6 monolayers of MgO calculated from the Δ_1-like band of the complex band structure of MgO via Eq. (5); the black circle marks the region with $|k_\parallel| < 0.1\frac{2\pi}{a_{\text{Fe}}}$ where 94 % of the transmission takes place

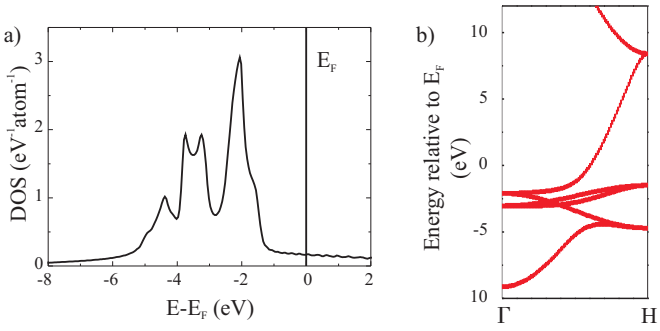

FIG. 8: a) Density of states of bcc-Cu with the lattice constant a_{Fe} of bcc-Fe b) band structure of bcc-Cu along ΓH (current direction)

iron (a-Fe) and bcc cobalt (bcc-Co) with the lattice structure of bcc-Fe ($a_{\text{Fe}} = 2.87$ Å). To estimate the polarization of the Δ_1-like states (P_{Δ_1}) and to investigate the influence of the finite thickness of the magnetic material we attach an effective non-magnetic material to the magnetic electrodes. This material has to serve as an electron reservoir with Δ_1-like states. For simplicity bcc-Cu is used with a lattice constant of bcc-Fe. The corresponding DOS shown in Fig. 8 (a) indicates that the d-states are occupied and the band structure in the current direction (see Fig. 8 (b)) shows a Δ_1 state at the Fermi level. Therefore, bcc-Cu is well suited to serve as a non - magnetic free electron like reservoir with Δ_1-like states close to the center of the BZ which causes optimal matching to the Δ_1-like states of the MgO barrier. Tunneling via Δ_1-like states is also important with respect to future applications since it guarantees a reasonably low resistance area product.

In addition to our previous article[25] where we analyzed bcc-Fe and a-Fe we also embed bcc-Co between bcc-Cu (see Fig. 9) to compare the transport properties. The results for the conductance calculations depending on the thickness of the magnetic layers are presented in Fig. 10. The thickness of the magnetic layer is measured in $a_{Fe}/2$ which is the monolayer spacing in crystalline Fe. Both crystalline magnets show a similar decay of the conductance with the thickness of the magnetic layer which

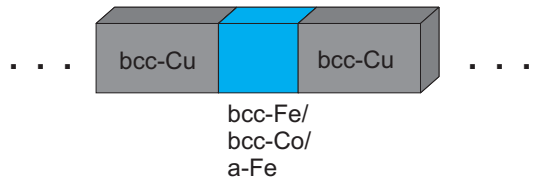

FIG. 9: Junction geometry for the calculations of the transport properties through different magnetic electrode materials

is different from that of amorphous Fe. While the conductance density remains nearly constant for the majority spin channel for bcc-Fe and bcc-Co the values for the minority spin decrease drastically with increasing number of crystalline monolayers.

This results in a spin polarization of the currents P_{Δ_1} through bcc-Fe and bcc-Co as high as 70 % (see Table I) with 4 magnetic monolayers only. The index Δ_1 indicates that the current carrying states are Δ_1-like triggered by the bcc-Cu reservoir. The value for P_{Δ_1} is in good agreement with the experimentally found polarization $P_{\rm exp}$(MgO)[17] for the tunneling current from bcc-Fe through MgO into a superconductor. In the amorphous Fe system the conductance values in the majority and the minority spin channel are comparable to each other and lie in between the values of the spin channels for the crystalline magnetic materials. The corresponding polarization P_{Δ_1} is as small as 14 %.

The TMR ratios calculated from P_{Δ_1} by the Julliere model (Eq. 4) are presented in Table I. For a-Fe the TMR ratio is negligible but with bcc-Fe and bcc-Co the TMR ratio reaches nearly 200 % with only 4 magnetic monolayers. This estimated TMR ratio is higher than the one obtained from the polarization based on the total DOS at the Fermi level[47,48] ($P_{\rm exp}(Al_2O_3)$), but is still drastically smaller than the predicted ratios for bcc-Fe[14,15] and bcc-Co[20] electrodes. The shortcoming of the estimation is that all $\mathbf{k}_{\|}$ states in the BZ contribute with equal weight since g is not in the tunneling regime. To account for the decay of the tunneling currents with increasing $k_{\|}$ due to the complex band structure of the MgO barrier, the estimation is further reduced to the states close to the center of the BZ. In particular, we use the effective polarization ($P_{\rm eff}$) introduced in Sec. III and Fig. 7.

To illustrate these regions where $P_{\rm eff}$ is calculated Fig. 11 shows the transmission maps of the crystalline junctions with 4 magnetic monolayers of bcc-Fe and bcc-Co in comparison to bcc-Cu for the BZ of the size $(2\pi/a_{\rm Fe}) \times (2\pi/a_{\rm Fe})$ which corresponds to the bcc(001) surface. The conductance map for bcc-Cu is identical in both spin channels since Cu is non-magnetic. The results for bcc-Fe and bcc-Co are similar to each other. The contributions of the majority spin direction are comparable to the values of bcc-Cu. In contrast, the contributions of the minority spin direction are very small and indicate especially around the center of the Brillouin zone, a low transmission probability like in a tunneling regime. This

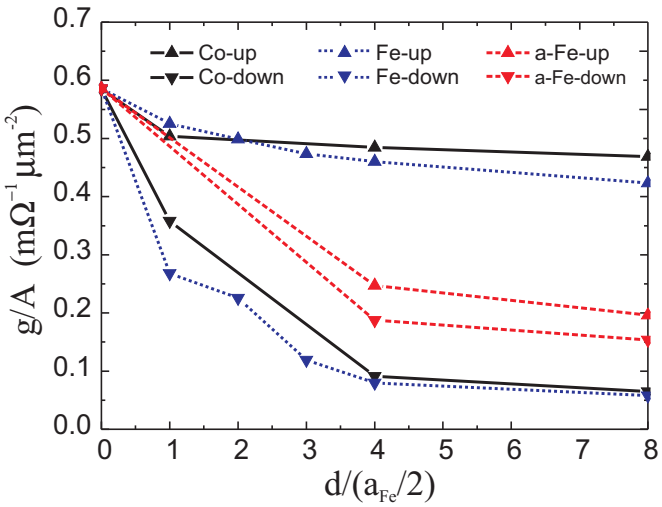

FIG. 10: Conductance densities for the analyzed magnetic materials embedded between semi-infinite bcc-Cu

is consistent with the band structure of bcc-Fe and bcc-Co in a bulk structure as discussed by Zhang et al.[20] and Yuasa et al..[10]

For a quantitative analysis, the effective spin polarization $P_{\rm eff}$ of the current is presented in Table I. With 4 monolayers, the calculated polarization is as high as 98 % and 86 % for bcc-Fe and bcc-Co, respectively. Applying Eq. (4) TMR ratios of 4850 % and 568 % are expected already for thin magnetic layers of bcc-Fe and bcc-Co. These ratios are significantly higher than the values based on the spin polarization of all Δ_1-like states (P_{Δ_1}) and are comparable to the *ab initio* calculated TMR ratios of systems with semi-infinite magnetic electrodes.[14,15,20]

For a comparison of these results to a system with a-Fe as magnetic electrode it is important to consider the different size of the BZ. As mentioned before the BZ of the amorphous system has a size of $(\pi/a_{\rm Fe})\times(\pi/a_{\rm Fe})$ because of the larger unit cell. In principle, the calculations for the crystalline system can be performed with a unit cell of larger size to enable comparison of the conductance maps $T^{\sigma}(k_{\|})$ in the reduced BZ of the amorphous system. Fig. 12 (a) illustrates the down-folding of the larger BZ (left) into the smaller one $(\pi/a_{\rm Fe})\times(\pi/a_{\rm Fe})$ where two additional points of the BZ boundary are folded into the BZ center. This procedure is mathematically correct but information concerning the transmission, in particular, the symmetry selection got lost. Obviously, one can no longer distinguish between the states originally occurring at the BZ center $\bar{\Gamma}$ and the ones down-folded from the BZ boundary. But in a crystalline tunnel junction with a MgO barrier only those states which are originally at the $\bar{\Gamma}$-point can match to the states with the lowest decay rates of the MgO. For a-Fe (see Fig. 12 (b)) the symmetry is reduced and all states at the BZ center can match to the MgO states with the lowest decay rate.

As a result of the structural disorder the transmission of all $\mathbf{k}_{\|}$ states is comparable for both spin directions.

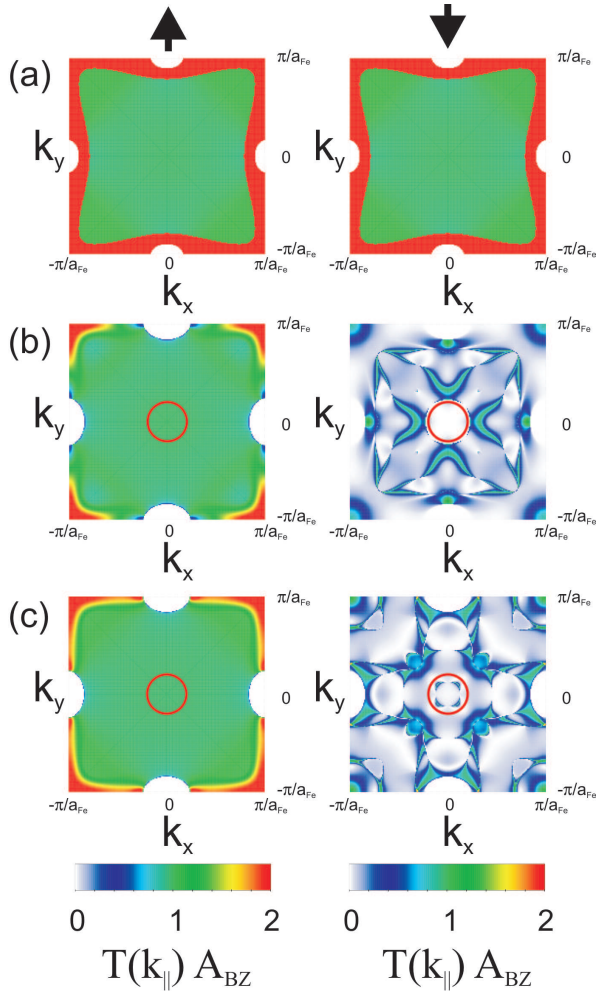

FIG. 11: Transmission maps $T^{\sigma}(k_{\|})$ for different crystalline magnetic electrode materials (thickness of the magnetic layer: 2 a_{Fe}):
(a) bcc-Cu/bcc-Cu
(b) bcc-Cu/bcc-Fe/bcc-Cu
(c) bcc-Cu/bcc-Co/bcc-Cu
Red circles indicate the region where the effective spin polarization P_{eff} is calculated.

The TMR ratio deduced from the effective spin polarization P_{eff} is 1 %. The effective spin polarization of -7 % of the lead material (see Table I) leads to a larger conductance for the minority spin channel in comparison with the majority spin channel in the parallel configuration of the real tunnel junction. (see Table I).

Our calculations predict that sub-nanometer bcc-Fe and bcc-Co layers are efficient spin-filters for Δ_1-like states and promising candidates to yield a high TMR ratio in contact with a MgO barrier. In the next section we compare our predictions based on the spin polarizations of currents through different magnetic materials to our results of *ab initio* calculations of special tunnel junctions.

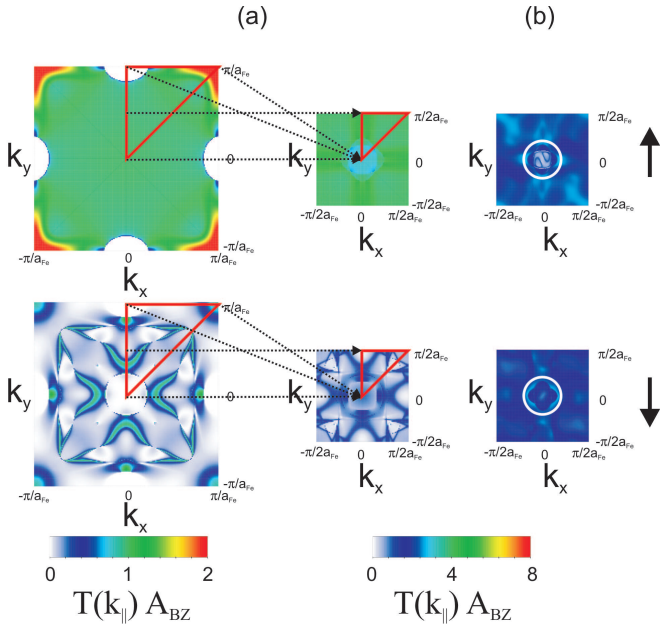

FIG. 12: Comparison of the transmission maps of bcc-Fe and a-Fe for the analysis as magnetic electrode materials (thickness of the magnetic layer: 2 a_{Fe}):
(a) bcc-Cu/bcc-Fe/bcc-Cu
(b) bcc-Cu/a-Fe/bcc-Cu
White circles indicate the region where the effective spin polarization P_{eff} is calculated (see Table I).

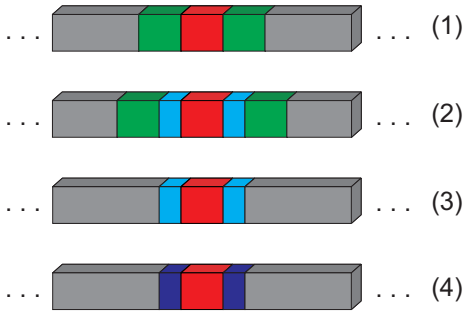

FIG. 13: model tunnel junctions:
(1) bcc-Cu/a-Fe/MgO/a-Fe/bcc-Cu
(2) bcc-Cu/a-Fe/bcc-Fe/MgO/bcc-Fe/a-Fe/bcc-Cu
(3) bcc-Cu/bcc-Fe/MgO/bcc-Fe/bcc-Cu
(4) bcc-Cu/bcc-Co/MgO/bcc-Co/bcc-Cu

V. TUNNEL JUNCTIONS WITH FINITE FERROMAGNETIC LAYERS

In this section we investigate different tunnel junctions to quantify the conclusions from the properties of the electrode materials in the last section. This means that now the role of the interface between magnetic layer and barrier and the whole complex band structure of the barrier is included in *ab initio* calculations. To take the finite thickness of the magnetic layer into account, the reservoirs are again semi-infinite bcc-Cu electrodes

TABLE I: Transport properties of bcc-Fe, bcc-Co, and amorphous Fe with a thickness of 2 a_{Fe} embedded between semi-infinite bcc-Cu, and corresponding TMR ratios. The following different polarizations are used to estimate the TMR ratio in the Julliere model using Eq. (4).
P_{exp} (Al_2O_3): spin polarization of a ferromagnet (FM) measured in a (FM/amorphous Al_2O_3/superconductor) tunnel junction[47,48]
P_{exp} (MgO): spin polarization of a ferromagnet (FM) measured in a (FM/MgO/superconductor) tunnel junction[17]
P_{Δ_1}: spin polarization of Δ_1-like states (this article) by using a reservoir which provides only Δ_1-like states
P_{eff}: effective spin polarization of Δ_1-like states in a region of the BZ with $|\mathbf{k}_{\parallel}| < 0.1\frac{2\pi}{a_{\mathrm{Fe}}}$ (marked with circles in Fig. 11) where the main contribution to the total tunneling current is expected (see Fig. 7)
tunnel junctions (*ab initio*): *ab initio* calculation of the TMR ratio of the full tunnel junctions (see Sec. V). The geometries used are (3) and (4) in Fig. 13 for bcc-Fe and bcc-Co with 4 monolayers. For the amorphous Fe the junction geometry (1) is used without any crystalline magnetic layer

	Julliere model								**tunnel junctions *ab initio***
	P_{exp}[47] (Al_2O_3)	TMR ratio	P_{exp}[17] (MgO)	TMR ratio	P_{Δ_1}	TMR ratio	P_{eff}	TMR ratio	TMR ratio
bcc-Fe	44 %	48 %	74 %	242 %	70 %	192 %	98 %	4850 %	8800 %
bcc-Co	34 %	26 %			68 %	172 %	86 %	568 %	900 %
a-Fe					14 %	4 %	-7 %	1 %	44 %

as sketched in Fig. 13. The barrier consists of 6 monolayers MgO which acts as a symmetry filter for Δ_1-like states as mentioned above. The junction geometry (1) is given by amorphous ferromagnetic layers with the thickness of 2 a_{Fe} adjacent to the barrier. In a second step, a finite number of bcc-Fe monolayers is inserted between the barrier and the amorphous Fe denoted as junction (2) in Fig. 13. The influence of the amorphous Fe in a junction with relatively many bcc-Fe monolayers is discussed by omitting the amorphous layer getting the junction geometry (3). This junction will be compared to a junction with bcc-Co instead of bcc-Fe sketched as (4). The effective Kohn-Sham potentials of all structures are calculated self-consistently.

As expected from the transport properties of amorphous Fe (see Table I), the TMR effect is very small with only amorphous iron as magnetic electrode material. In the Julliere model we estimate about 1 %. In the *ab initio* calculation we calculate a TMR ratio of 44 %. The small TMR ratio is due to the very low spin polarization (P_{Δ_1}=14 %) and the similar behavior for both spin channels around the center of the BZ. Obviously, the self-consistent treatment of the interface structure leads to a higher TMR ratio but the lack of a high P_{eff} drastically restricts the achievable TMR ratio.

As discussed in our previous article[25] it turned out that inserting two monolayers of crystalline Fe between the MgO (see Fig. 13 (2)) and the amorphous layers is sufficient to recreate a TMR ratio as high as 2900 %, which is comparable to the system with semi-infinite crystalline Fe electrodes (see Fig. 14). In such a system the crystalline Fe causes a high effective spin polarization P_{eff} for the Δ_1-like states close to the center of the BZ as discussed in the previous section. There we estimate the TMR ratio with 4 crystalline magnetic layers to be 4850 %. Now we calculate 8800 % (see Table I) for the real tunnel junction which shows that the estimation works well.

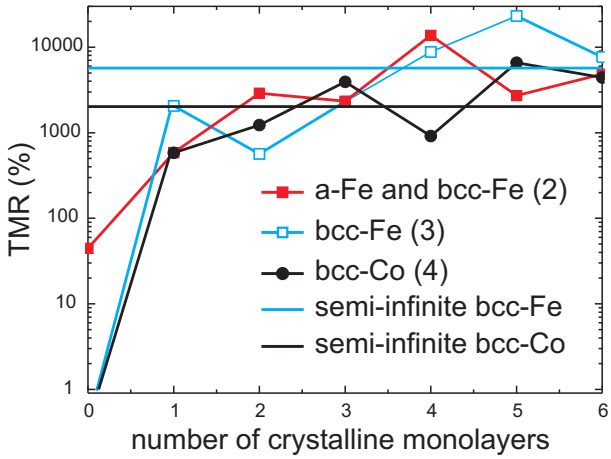

FIG. 14: TMR ratio in dependence on the number of crystalline Fe layers next to the barrier for the model tunnel junctions sketched in Fig. 13

The increase of the polarization from a-Fe to bcc-Fe gives rise to these high TMR ratios. Therefore, the question of the influence of a-Fe arises when there are a couple of bcc-Fe monolayers between the barrier and a-Fe. For this purpose we compare in Fig. 14 the junctions with and without an a-Fe layer. The influence of the amorphous Fe is negligible if more than 2 crystalline Fe monolayers are inserted.

For a system with bcc-Co electrodes structural disorder is not considered and the results are similar to the case of crystalline Fe. For both systems a high TMR ratio has been found with magnetic electrodes of only one crystalline monolayer thickness and with 3 monolayers the TMR ratio is comparable to the results of semi-infinite electrodes. The stronger oscillations with the thickness of

the ferromagnetic layer in the bcc-Co system result from sharp resonance effects in the minority spin channel of the parallel configuration.

In contrast to other theoretical results[20] we found lower values for the TMR ratio (2000 %) for semi-infinite bcc-Co electrodes than in a system with bcc-Fe (6000 %). The reason can be attributed to different structural data of the interface. In the present paper the experimentally obtained bcc-Fe/MgO/bcc-Fe structure[50,51] was used for both the bcc-Fe and the bcc-Co system. The explanation for the high TMR ratio given by Zhang et al.[20] is restricted to the $\bar{\Gamma}$ point only. There the majority spin channel of bcc-Co has only Δ_1 symmetry and no other states occur, whereas in bcc-Fe states with Δ_5 and Δ_2 symmetry exist. This leads for bcc-Co to a total reflection of all states in the antiparallel configuration at the $\bar{\Gamma}$ point. This behavior occurs also in the present calculation where no contributions in both spin channels of the antiparallel configuration at the $\bar{\Gamma}$ point exist. But around the $\bar{\Gamma}$ point non-negligible contributions have been found, which leads to a finite, quite high TMR ratio.

VI. CONCLUSION

The results of this paper demonstrate that the magnitude of the TMR effect can strongly be manipulated by structure and geometry of the ferromagnetic electrode. We showed that a detailed analysis of the spin-dependent transport properties of the magnetic layers considering the symmetry selection properties of MgO is sufficient to estimate the expected TMR ratio of a tunnel junction. If the symmetry selection of the barrier, following from the complex band structure of the bulk material, is known, a similar procedure can be used for other tunnel junctions with different crystalline barriers. We estimate the TMR ratio of a MgO based tunnel junction by calculating the spin-dependent transport properties through different magnetic layers (a-Fe, bcc-Fe, bcc-Co) embedded between non-magnetic bcc-Cu reservoirs. In particular, we analyze the spin filter effect of the magnetic layers by calculating an effective polarization. We verify these estimations by *ab initio* calculations of the complete tunnel junctions. It turned out that bcc-Co and bcc-Fe as thin magnetic layers show similar behavior and even 1 monolayer is sufficient to create a high TMR ratio. The influence of an amorphous layer in addition to a crystalline ferromagnetic layer is negligible. In contrast, with an electrode of amorphous-Fe in direct contact with MgO the TMR effect is suppressed.

Acknowledgments

This work has been supported in part by the NIST-CNST/UMD-NanoCenter Cooperative Agreement. Financial support by the DFG (No. FG 404) is kindly acknowledged.

* Electronic address: martin.gradhand@physik.uni-halle.de
† Electronic address: christian.heiliger@nist.gov

[1] J. S. Moodera, L. R. Kinder, T. M. Wong, and R. Meservey, Phys. Rev. Lett. **74**, 3273 (1995).
[2] T. Miyazaki and N. Tezuka, J. Magn. Magn. Mater. **139**, L231 (1995).
[3] M. Julliere, Phys. Lett. A **54**, 225 (1975).
[4] S. Baea, J. H. Judy, I.-F. Tsu, and M. Davis, J. Appl. Phys. **94**, 7636 (2003).
[5] J.-G. Zhu and C. Park, Mater. Today **9**, 36 (2006).
[6] S. S. P. Parkin, K. P. Roche, M. G. Samant, P. M. Rice, R. B. Beyers, R. E. Scheuerlein, E. J. O'Sullivan, S. L. Brown, J. Bucchigano, D. W. Abraham, et al., J. Appl. Phys. **85**, 5828 (1999).
[7] S. A. Wolf, A. Y. Chtchelkanova, and D. M. Treger, IBM J. RES. & DEV. **50**, 101 (2006).
[8] S. Ikeda, J. Hayakawa, Y. M. Lee, R. Sasaki, T. Meguro, F. Matsukura, and H. Ohno, Jpn. J. Appl. Phys. **44**, L1442 (2005).
[9] S. Parkin, MRS Bulletin **31**, 389 (2006).
[10] S. Yuasa, A. Fukushima, H. Kubota, Y. Suzuki, and K. Ando, Appl. Phys. Lett. **89**, 042505 (2006).
[11] J. Hayakawa, S. Ikeda, Y. Lee, F. Matsukura, and H. Ohno, Appl. Phys. Lett. **89**, 232510 (2006).
[12] Y. Lou, M. Esseling, A. Käufler, K. Samwer, T. Dimopoulos, G. Gieres, M. Vieth, M. Rührig, J. Wecker, C. Rudolf, et al., Phys. Rev. B **72**, 014426 (2005).
[13] L. Yuan, S. H. Liou, and D. Wang, Phys. Rev. B **73**, 134403 (2006).
[14] J. Mathon and A. Umerski, Phys. Rev. B **63**, 220403 (2001).
[15] W. Butler, X.-G. Zhang, T. Schulthess, and J. MacLaren, Phys. Rev. B **63**, 054416 (2001).
[16] D. D. Djayaprawira, K. Tsunekawa, M. Nagai, H. Maehara, S. Yamagata, N. Watanabe, S. Yuasa, Y. Suzuki, and K. Ando, Appl. Phys. Lett. **86**, 092502 (2005).
[17] S. S. P. Parkin, C. Kaiser, A. Panchula, P. M. Rice, B. Hughes, M. Samant, and S. H. Yang, Nat. Mat. **3**, 862 (2004).
[18] X.-G. Zhang, W. H. Butler, and A. Bandyopadhyay, Phys. Rev. B **68**, 092402 (2003).
[19] D. Wortmann, G. Bihlmayer, and S. Blgel, J. Phys.: Condens. Matter **16**, 5819 (2004).
[20] X.-G. Zhang and W. H. Butler, Phys. Rev. B **70**, 172407 (2004).
[21] C. Heiliger, P. Zahn, B. Y. Yavorsky, and I. Mertig, Phys. Rev. B **72**, 180406 (R) (2005).
[22] K. Belashenko, J. Velev, and E. Tsymbal, Phys. Rev. B **72**, 140404 (2005).
[23] J. Mathon and A. Umerski, Phys. Rev. B **74**, 140404 (2006).
[24] H. Itoh, J. Phys. D **40**, 1228 (2007).
[25] C. Heiliger, M. Gradhand, P. Zahn, and I. Mertig, Phys.

Rev. Lett. **99**, 066804 (2007).
[26] R. Zeller, P. Dederichs, B. Ujfalussy, L. Szunyogh, and P. Weinberger, Phys. Rev. B **52**, 8807 (1995).
[27] N. Papanikolaou, R. Zeller, and P. H. Dederichs, J. Phys.: Condens. Matter **14**, 2799 (2002).
[28] H. U. Baranger and A. D. Stone, Phys. Rev. B **40**, 8196 (1989).
[29] P. Mavropoulos, N. Papanikolaou, and P. H. Dederichs, Phys. Rev. B **69**, 125104 (2004).
[30] R. Landauer, Z. Phys. B **68**, 217 (1987).
[31] B. Wenzien, J. Kudrnovsky, V. Drchal, and M. Sob, J. Phys.: Condens. Matter **1**, 9893 (1989).
[32] M. P. L. Sancho, J. M. L. Sancho, and J. Rubio, J. Phys. F **15**, 851 (1985).
[33] M. R. Bennet and J. G. Wright, Phys Status Solidi A **13**, 135 (1972).
[34] T. Ichikawa, Phys. Status Solidi A **19**, 707 (1973).
[35] P. K. Leung and J. G. Wright, Phil. Mag. **30**, 995 (1974).
[36] R. V. Aldridge and S. J. Raeburn, Phys. Lett. A **56**, 211 (1976).
[37] J. G. Wright, Liquid Metals (Inst. Phys. Conf.) **30**, 251 (1977).
[38] S. J. Raeburn and R. V. Aldridge, J. Phys. F **8**, 1917 (1978).
[39] C. L. Chien and K. M. Unruh, Phys. Rev. B **24**, 1556 (1981).
[40] R. Bellissent, G. Galli, M. W. Grinstaff, P. Migliardo, and K. S. Suslick, Phys. Rev. B **48**, 15797 (1993).
[41] M. Liebs and M. Fähnle, Phys. Rev. B **53**, 14012 (1996).
[42] I. Turek and J. Hafner, Phys. Rev. B **46**, 247 (1992).
[43] R. Lorenz and J. Hafner, J. Magn. Magn. Mater. **139**, 209 (1995).
[44] M. Liebs, K. Hummler, and M. Fähnle, Phys. Rev. B **51**, 8664 (1995).
[45] O. Y. Kontsevoi and V. A. Gubanov, Phys. Rev. B **51**, 15125 (1995).
[46] B. Y. Yavorsky and I. Mertig, Phys. Rev. B **74**, 174402 (2006).
[47] P. Tedrow and R. Meservey, Phys. Rev. B **7**, 318 (1973).
[48] R. Meservey and P. Tedrow, Phys. Rep. **238**, 173 (1994).
[49] C. Heiliger, P. Zahn, and I. Mertig, Mater. Today **9**, 46 (2006).
[50] H. L. Meyerheim, R. Popescu, J. Kirschner, N. Jedrecy, M. Sauvage-Simkin, B. Heinrich, and R. Pinchaux, Phys. Rev. Lett. **87**, 076102 (2001).
[51] H. Meyerheim, R. Popescu, N. Jedrecy, M. Vedpathak, M. Sauvage-Simkin, R. Pinchaux, B. Heinrich, and J. Kirschner, Phys. Rev. B **65**, 144433 (2002).